Small-particle composites. I. Linear optical properties

V. A. Markel* and Vladimir M. Shalaev†
Department of Physics, New Mexico State University, Las Cruces, New Mexico 88003

E. B. Stechel
Sandia National Laboratories, Albuquerque, New Mexico 87185

W. Kim and R. L. Armstrong
Department of Physics, New Mexico State University, Las Cruces, New Mexico 88003
(Received 21 February 1995; revised manuscript received 22 June 1995)

Absorption and extinction spectra of fractal and nonfractal small-particle composites are studied. General solutions of the coupled-dipole equations with the exact operator for the dipole interaction (including the near-, intermediate-, and far-zone terms) are found and compared with those in the quasistatic approximation. Broad-scale numerical simulations of optical spectra for clusters containing a large number of particles (up to 10 000) are performed. A significant fraction of dipolar eigenmodes in fractal aggregates is shown to be strongly localized. The eigenmodes cover a wide spectral region providing resonant enhancement in the visible and infrared parts of the spectrum. In contrast to previous predictions, the absorption spectrum is shown to be significantly different from the spectral distribution of the density of dipole eigenmodes. It clearly indicates the importance of symmetry properties of the modes and corresponding selection rules for the absorption by different modes in random fractal composites. Our experimental data obtained for extinction spectra of silver colloid fractal aggregates are in good agreement with the results of numerical simulations.

I. INTRODUCTION

Electromagnetic phenomena in inhomogeneous metal-insulator composites (thin films, cermets, colloidal aggregates, etc.) have been intensively studied for the last two decades.[1] Such nanostructured composites possess fascinating electromagnetic properties, which differ greatly from those of ordinary bulk material, and they are likely to become ever more important with the miniaturization of electronic components.

Fractal structures are prevalent in composites. The emergence of fractal geometry was a significant breakthrough in the description of irregularity.[2] Fractal objects (fractals) do not possess translational invariance and, therefore, cannot transmit ordinary waves.[2,3] Accordingly, dynamical excitations such as vibrational modes (fractons) tend to be localized in fractals.[2,3] Formally, this is a consequence of the fact that plane running waves are not eigenfunctions of the operator of dilation symmetry characterizing fractals. The efficiency of fractal structures in damping running waves is probably the key to a "self-stabilization" of many of the fractals found in nature.[2]

Dipolar eigenmodes in fractal composites are substantially different from those in other media. For example, there is only one dipolar eigenstate that can be excited by a homogeneous field in a dielectric sphere;[4] the total dipole moment of all other eigenstates is zero and, therefore, they can be excited only by inhomogeneous field. In contrast, fractal aggregates possess a variety of dipolar eigenmodes, distributed over a wide spectral range, which can be excited by a homogeneous field. In the case of continuous media, dipolar eigenstates (polaritons) are running plane waves that are eigenfuctions of the operator of translational symmetry. This also holds in most cases for microscopically disordered media that are, on average, homogeneous. Dipolar modes, in this case, are typically delocalized over large areas, and all monomers absorb light energy, with approximately equal rate, in regions that significantly exceed the wavelength. In contrast, fractal composites have eigenstates that are often localized in subwavelength regions. Absorption by monomers in these "hot zones" is much higher than by other monomers in a fractal composite. This is a consequence of the already mentioned fact that fractals do not posses translational symmetry; instead, they are symmetrical with respect to scale transformation.

The localization of optical eigenmodes, and associated strong field fluctuations can lead to a dramatic enhancement of many optical effects in fractals.[5–7] The theory of optical excitations in fractal clusters and percolation systems has been under development during the last decade, in particular, by Berry,[8] Stroud,[9] Bergman,[10] Fuchs and Claro,[11] Devaty,[12] Brouers,[13] Niklasson,[14] and by Markel, Stockman, Shalaev and their co-workers.[5–7,15–26] Strong localization of dipolar eigenmodes in regions smaller than the wavelength was predicted in Ref. 15, demonstrated by numerical simulations in Ref. 18 and experimentally observed in Ref. 25; independently, localization of optical modes was also studied in Refs. 9 and 13, using a resistor-inductor-capacitor network model. (Note that along with localized modes in fractals, there are delocalized ones as well.) Localized modes produce high-local-field ("hot") zones resulting in strong enhancement of optical phenomena, such as Rayleigh,[17] Raman,[19] and, especially, nonlinear light scattering.[22–24] In fractal aggregates composed of metal nanoparticles and in rough self-affine films, these modes are associated with localized surface plasmon (LSP) oscillations.

Strong localization of eigenmodes leads to a patchwork-like distribution of local fields associated with "hot" and "cold" zones in fractals. This brings about large spatial fluctuations of local fields in fractal composites and huge enhancement of various optical effects.

An important property of the interaction of light with fractals is the strong frequency and polarization dependence of the spatial location of light-induced dipole modes.[7,23,25] Such frequency-spatial and polarization-spatial selectivity may lead, in particular, to persistent holes induced by laser radiation in the spectra of fractals;[23] such behavior could find applications in the recording and processing of optical information. This selectivity arises because fractal morphology results in localization of optical modes on different parts of an object with random local structure.

General understanding of the properties briefly outlined above has been achieved during the past few years. However, most of these properties have been verified only for the binary model[5,6,15] and for the model of diluted aggregates[27] with a relatively small number of particles.[15–19,24,26] Although these two models allow qualitative predictions of most of the basic properties of fractals, as a rule, they cannot quantitatively describe optical excitations of real self-supporting aggregates that often consist of many thousands of particles. In addition, all previous considerations (except Ref. 17) were restricted to the quasistatic approximation. Broad-scale numerical simulations presented in a recent paper,[26] although including simulations for nondiluted clusters, were still limited to clusters of only 100–300 particles in the quasistatic approximation.

In this paper we go beyond these limitations. We find general solutions of the coupled-dipole equations with the exact operator for the dipole interaction (including the near-, intermediate-, and far-zone terms). Also, we report results from simulations for clusters consisting of large numbers of particles, from 500 to 10 000. This allows us to check the basic predictions of previously developed theories and to discover new properties of fractal aggregates. We show, in particular, that the spectral dependence of absorption by fractals significantly differs from that of the density of dipolar eigenmodes; in contrast to previous predictions.[15,16,26] This indicates the importance of symmetry properties of dipole modes in absorption by random fractals. Our numerical simulations also demonstrate a significant difference in absorption spectra of fractal and nonfractal composites.

In Sec. II we present the basic equations describing dipole excitations of a small-particle aggregate and discuss some of their general properties. Section III describes the numerical methods and models used in our simulations. Within the quasistatic approximation, the results of numerical simulations for absorption, spectral density, and eigenstate localization length are presented in Sec. IV. (We consider here optical properties of various fractal clusters and compare them with those for nonfractal aggregates.) In Sec. V we present numerical calculations of extinction spectra of silver colloid fractal aggregates, obtained within both the quasistatic approximation and the λ-dependent dipole interaction (where λ is the wavelength), and compare these simulations with experimental aggregate spectra. Sec. VI summarizes and discusses our results.

II. COUPLED-DIPOLE EQUATIONS AND OPTICAL CROSS SECTIONS

We consider the interaction of a plane electromagnetic wave $\mathbf{E}(\mathbf{r},t)=\mathbf{E}^{(0)}\exp(i\mathbf{k}\cdot\mathbf{r}-i\omega t)$ with a cluster of N particles (monomers) located at points $\mathbf{r}_1,\ldots,\mathbf{r}_N$. The monomers are assumed to be spherical with diameter much less than the wavelength of light. The particles are polarizable, with light-induced dipoles given by $\mathbf{d}_i=\alpha_0\mathbf{E}_i$, where $\mathbf{E}_i$ is the local field acting on the ith particle of isotropic polarizability α_0. The local field at any point is a superposition of the incident wave and all secondary waves scattered by the dipoles. Thus, dipole moments interact with each other and with the incident field, and obey the coupled-dipole equations (CDE's):

$$d_{i\alpha}=\alpha_0\left(E_\alpha^{(0)}\exp(i\mathbf{k}\cdot\mathbf{r}_i)+\sum_{j=1}^{N}{}' G_{\alpha\beta}(\mathbf{r}_{ij})d_{j\beta}\right), \quad (1)$$

where the time-dependent term, $\exp(-i\omega t)$, is omitted, $\mathbf{r}_{ij}=\mathbf{r}_i-\mathbf{r}_j$, and Σ' denotes the sum over all values of index j except $j=i$. The interaction tensor $G_{\alpha\beta}$ is defined as

$$G_{\alpha\beta}(\mathbf{r})=k^3\left(A(kr)\delta_{\alpha\beta}+B(kr)\frac{r_\alpha r_\beta}{r^2}\right), \quad (2)$$

$$A(x)=[x^{-1}+ix^{-2}-x^{-3}]\exp(ix), \quad (3)$$

$$B(x)=[-x^{-1}-3ix^{-2}+3x^{-3}]\exp(ix), \quad (4)$$

where α (should not be confused with the polarizability α) and β denote Cartesian components. Summation over repeated Greek indices is implied.

Following Refs. 15 and 16, we introduce a $3N$-dimensional complex vector space C^{3N} and an orthonormal basis $|i\alpha)$. Vectors $|d)$ and $|E)\in C^{3N}$, and their components in this basis are $(i\alpha|d)=d_{i,\alpha}$ and $(i\alpha|E)=E_{i,\alpha}=E_\alpha^{(0)}\exp(i\mathbf{k}\cdot\mathbf{r}_i)$. Similarly, we introduce a $3N\times 3N$ operator $\hat{V}$, which in the $|i\alpha)$ basis, has components $(i\alpha|\hat{V}|j\beta)=-G_{\alpha\beta}(\mathbf{r}_{ij})$ where $G_{\alpha\beta}(\mathbf{r}_{ij})$ is defined in (2)–(4). Then, Eq. (1) acquires the form of a matrix equation:

$$(Z+\hat{V})|d)=|E), \quad (5)$$

where $Z=1/\alpha_0$. Note that, generally, $\hat{V}$ is symmetric but not Hermitian (see also Ref. 28).

As shown in the Appendix the solution of (5) has the form

$$|d)=\sum_n \frac{|n)(\bar{n}|E)}{(\bar{n}|n)}\frac{1}{Z+v_n}, \quad (6)$$

where v_n are eigenvalues of $\hat{V}$, defined by $\hat{V}|n)=v_n|n)$, and the "bar" denotes complex conjugation of all components of a vector. Thus, if $|n)$ is a column vector, $(\bar{n}|$ is a row vector with the same entries as $|n)$. Although the $|n)$ basis is not, in general, orthogonal it can be shown that $(\bar{m}|n)=0$ for $m\neq n$ (see the Appendix).

In the $|i\alpha)$ basis, the solution (6) obviously acquires the form

$$d_{i,\alpha}=\sum_{n,j}\frac{(i\alpha|n)(\bar{n}|j\beta)E_{j,\beta}}{[\Sigma_{i'}(\bar{n}|i'\alpha')(i'\alpha'|n)]}\frac{1}{Z+v_n}. \quad (7)$$

Formulas (6) and (7) generalize solutions of the CDE's previously obtained in the quasi-static limit (see, for example, Refs. 15 and 16) to the case of the λ-dependent dipolar interaction. According to (6)–(7), for an arbitrary collection of N interacting particles, there are $3N$ eigenmodes with resonant eigenfrequencies defined by $\mathrm{Re}(Z)+v_n=0$. The weight with which a mode contributes to the resultant optical response depends on the scalar product $(\bar{n}|E)$ and, thus, on symmetry properties of the eigenvectors $|n)$.

Once the CDE's (1) are solved for dipole moments $\mathbf{d}_i$, extinction, absorption, and scattering cross sections (σ_e, σ_a, and σ_s, respectively) can be obtained from the optical theorem[29,30]

$$\sigma_e=4\pi k|E^{(0)}|^{-2}\mathrm{Im}\sum_{i=1}^{N} d_{i\alpha}E_\alpha^{(0)*}\exp(-i\mathbf{k}\cdot\mathbf{r}_i)$$

$$=4\pi k|E^{(0)}|^{-2}\mathrm{Im}(d|E), \tag{8}$$

$$\sigma_a=4\pi k|E^{(0)}|^{-2}y_a\sum_{i=1}^{N}|d_i|^2=4\pi k|E^{(0)}|^{-2}y_a(d|d), \tag{9}$$

where

$$y_a=-\mathrm{Im}(Z)-2k^3/3 \tag{10}$$

is a non-negative constant characterizing the absorption strength. (The scattering cross section σ_s is defined by $\sigma_s=\sigma_e-\sigma_a$.) Note that each term in the sum (9) characterizes absorption by a single monomer, however, individual terms in the sum (8) have no independent physical significance, since scattering (and, therefore, extinction) is, in general, a collective phenomenon.

If clusters are much smaller than the wavelength of the incident wave and $y_a\gg 2k^3/3$,[31] one can use the quasistatic limit for the dipole interaction matrix. This means that one can omit terms $1/x$, $1/x^2$, and $\exp(ix)$ in (3), (4) and put $\exp(\pm i\mathbf{k}\cdot\mathbf{r}_i)=1$ in formulas (1) and (8). We use below the notations, $\hat{W}$ and w_n, for the quasistatic limits of the interaction operator and its eigenvalues. After averaging over the orientations of a cluster, the extinction cross section is expressed as

$$\sigma_e=4\pi kN\ \mathrm{Im}\alpha, \tag{11}$$

where

$$\alpha=(1/3N)\sum_i \mathrm{Tr}[\alpha_{\alpha\beta}^{(i)}]=(1/3N)\sum_i \alpha_{\alpha\alpha}^{(i)}, \tag{12}$$

and $\alpha_{\alpha\beta}^{(i)}$ is related to $d_{i\alpha}$ via

$$d_{i\alpha}=\alpha_{\alpha\beta}^{(i)}E_\beta^{(0)}. \tag{13}$$

The $d_{i\alpha}$ are to be found from the solution of (1). Thus, with the trivial prefactor $4\pi kN$, the extinction cross section is proportional to $\mathrm{Im}\alpha$.

We also define three normalized vectors, one for each direction $\alpha=x,y,z$ as follows:

$$|\phi_\alpha)=\frac{1}{\sqrt{N}}\sum_i |i\alpha).$$

Then, it is easy to show that

$$\alpha=\left(\phi_\alpha\left|\frac{1}{\hat{W}+Z}\right|\phi_\alpha\right)=\sum_n \frac{(\phi_\alpha|n)(n|\phi_\alpha)}{\alpha_0^{-1}+w_n}. \tag{14}$$

The basic formulas (7)–(14) presented in this section will be applied later to numerical simulations of optical properties of fractal composites.

III. NUMERICAL SIMULATIONS FOR SMALL-PARTICLE AGGREGATES

The CDE's (1) are general in the sense that they place no restrictions on the geometry of the aggregates. In particular, the system of equations (1) can be used to find the optical response of a fractal particle aggregate. In this case the number of monomers N and the radius of gyration of a cluster R_c are related by the well-known expression $N=(R_c/R_0)^D$, where R_0 is a length constant characterizing the separation between nearest neighbors and D is the fractal (Hausdorff) dimension. Note that, for fractals, the volume fraction occupied by particles, $p\sim N^{1-3/D}$, which $\to 0$ with increasing N. The density-density correlation function in fractals has a power-law dependence, $g(r)\propto r^{D-d}$, $D<d$, where d is the dimension of the embedding space ($d=3$ in our case) and r is the distance between two points in a cluster. This function increases with decreasing r. Thus, in fractals, despite the asymptotically zero mean density, there are always particles in close proximity, $\sim R_0$, to a given one, i.e., the interaction between particles is anticipated to be strong.

We have conducted numerical simulations of both fractal and nonfractal aggregates. Below we will briefly describe the computer models used to generate these small-particle aggregates.

Cluster-cluster aggregates (CCA) were built on a cubic lattice with periodic boundary conditions using a well-known numerical algorithm (see, for example, Ref. 33). The fractal dimension of CCA embedded in three-dimensional space is $D\approx 1.78$, and the length constant $R_0\approx a/3$, where a is the lattice period (equal to the particle diameter). We generated various assemblies of CCA's consisting of different numbers of particles, $N=500$, 1000, and 10 000. Note that the CCA model provides excellent simulation of empirically observed metal particles aggregates in solution.[34] In this model, encounters of randomly walking particles result in their sticking together, first to form small groups, which then aggregate into larger formations, and so on.

We also simulated other types of fractals, namely, Witten-Sander aggregates (WSA's) and random-walk aggregates (RWA's). WSA's result from diffusion-limited cluster-particle aggregation and have fractal dimension $D\approx 2.5$ (for details see, for example, Ref. 35). RWA's were generated based on the model of self-avoiding random walks; the fractal dimension in this case is $D\approx 1.7$. WSA's were built on a simple cubic lattice while RWA's were off lattice.

To compare fractal and nonfractal composites we also simulated a random gas of particles (RGP) and a close-packed sphere of particles (CPSP). In both cases $D=d=3$ and the correlation function $g(r)$ is constant. Particles were assumed to be hard spheres. To provide better comparison

with CCA, the RGP was generated in a spherical volume that would be occupied by a CCA with the same number of particles. This means that particles in CCA and RGP fill the same volume fraction, p (p was small, $p \approx 0.05$ for $N=500$). In RGP, distances between particles were random.

The CPSP was simulated in a spherical volume by randomly placing monomers (one by one) inside the volume. If placing a new monomer resulted in geometrical intersection with other particles, the trial was rejected. The process was stopped when a large number of trials were rejected. This algorithm allows one to achieve a fairly dense packing of spherical particles. For example, $N=500$ particles can be packed in a spherical volume $V=600$ with the radius $R_c=5.2$ (the diameter of a hard sphere is $a=1$). This means that $p \approx 0.44$ (cf., for close-packed spheres on a cubic lattice $p \approx 0.52$; it can be smaller than 0.44 for some other types of lattice).

To solve (1) for the aggregates described above, we used three different numerical methods. The first is based on diagonalization of the interaction matrix.[15,17] This method can be applied in the quasistatic approximation when all terms of the interaction matrix, $\hat{V}$, in (2)–(4) are real, and do not depend on $k=\omega/c$ (this requirement is, of course, fulfilled when $R_c \ll \lambda$). Provided eigenvectors and eigenvalues are calculated, solutions can be obtained using this method, for any value of α_0.

The second algorithm used in our numerical calculations was the conjugate-gradient method.[29] It is not restricted to the quasi-static approximation, and allows use of the exact formulas (2)–(4) for the interaction matrix in numerical simulations. The main difficulty of this method arises from the need to repeat a numerically intensive part of calculation for each new value of α_0. However, beyond the quasistatic approximation, this difficulty cannot be avoided by any computational method.

The last method used in numerical simulations with the interaction $\hat{W}$ in the quasistatic limit was based on the Lanczos algorithm.[36] The diagonal Green's function element in (14) can be written as a continued fraction that formally terminates after $3N$ levels.[37] However, in practice it converges in much fewer levels, i.e., in L levels with $L \ll 3N$ (for large N):

$$\left(\phi_\alpha \left| \frac{1}{\hat{W}+Z} \right| \phi_\alpha\right) \approx \cfrac{1}{\eta_{0,\alpha}+Z-\cfrac{[\beta_{1,\alpha}]^2}{\eta_{1,\alpha}+Z-\cfrac{[\beta_{2,\alpha}]^2}{\cdots \eta_{L-1,\alpha}+Z-[\beta_{L,\alpha}]^2 g_0(Z)}}}.$$

The η's and β's are determined by the basic Lanczos recursion relation[36]

$$\beta_{j+1,\alpha}|u_{j+1,\alpha}) = [\hat{W}-\eta_{j,\alpha}]|u_{j,\alpha}) - \beta_{j,\alpha}|u_{j-1,\alpha}),$$

where $\beta_{0,\alpha} \equiv 0$, $|u_{0,\alpha}) \equiv |\phi_\alpha)$, $|u_{-1,\alpha}) \equiv 0$, $\beta_{j+1,\alpha}$ are chosen so that $(u_{j+1,\alpha}|u_{j+1,\alpha}) = 1$, $\eta_{j,\alpha} = (u_{j,\alpha}|\hat{W}|u_{j,\alpha})$, and $g_0(Z)$ is a terminator that we take as the Green's function for a constant chain: $g_0(Z) = (2b^2)^{-1}[a+Z-\sqrt{(a+Z)^2-4b^2}]$, where $a-2b=w_{\min}$ and $a+2b=w_{\max}$, with $w_{\min}$ ($w_{\max}$) being the minimum (maximum) eigenvalue of $\hat{W}$. These extremum eigenvalues are easily determined by diagonalizing the $L \times L$ symmetric tridiagonal matrix made up of the η's on the diagonal and the β's on the first off diagonal.

The computationally intensive part of this calculation is the matrix vector multiplication, i.e., the evaluation of the $3N \times 3N$ matrix $\hat{W}$ operating on a vector $|u)$ of length $3N$. We find that approximately 100 levels are sufficient to converge the diagonal elements of the polarizability tensor. Consequently, calculations with $N=10\,000$ may be performed on a workstation whereas diagonalization of a $30\,000 \times 30\,000$ matrix is clearly not feasible.

IV. OPTICAL PROPERTIES OF SMALL-PARTICLE COMPOSITES IN THE QUASISTATIC APPROXIMATION

General properties of the solutions of (1) in the quasistatic approximation were reported in Refs. 15 and 16. Here we present some formulas that are relevant to subsequent numerical calculations.

In the quasistatic approximation the interaction tensor $\hat{W}$ does not depend on $k=\omega/c$, and the only source of dependence of the cluster absorption ($\mathrm{Im}\alpha$) on ω is through the polarizability α_0 of an individual monomer. Following Refs. 5, 6, and 15, we introduce real, X, and imaginary, δ, parts of $Z=1/\alpha_0$ so that

$$Z=1/\alpha_0=-(X+i\delta). \tag{15}$$

Note that solutions of the CDE's (1) can be expressed in terms of X and δ for an arbitrary form of the polarizability α_0. Alternatively, defining α_0, one can always specify the frequency dependence of the spectral variable X and decay parameter δ. Thus, solutions of the CDE's, expressed in terms of X and δ, have universal character, while their specific frequency (or wavelength) dependence is determined by the corresponding frequency dependence of $\alpha_0=\alpha_0(\omega)$ (which, in general, depends on the specific particles aggregated into a cluster). For example, in the vicinity of an isolated resonance, the polarizability can be represented as

$$\alpha_0 = \frac{R_m^3 \omega_m}{(\omega_0-\omega)-i\Gamma}, \tag{16}$$

where ω_0 is the resonance frequency of an individual monomer, Γ is the resonance half-width, and ω_m, R_m are the characteristic excitation frequency and effective size of a particle (in particular, in a two-level model $R_m^3\omega_m = |d_{12}|^2/\hbar$, where d_{12} is the dipole moment of the transition). Then, $X=R_m^{-3}(\omega-\omega_0)/\omega_m$ and $\delta=R_m^{-3}(\Gamma/\omega_m)$ [the quantity $(R_m^3\delta)^{-1}$ is a quality factor of the resonance]. In Sec. V we will also specify X and δ for the important case where the particles are dielectric spheres.

As follows from (10) and (15), the decay constant δ is related to y_a by $\delta=y_a+2k^3/3$. Since we assume strong absorption, i.e., $2k^3/3 \ll y_a$, the approximation $\delta=y_a$ is valid within the precision of the quasistatic approximation. As was shown in Ref. 15, an exact property of the CDE's solutions in the quasistatic approximation is

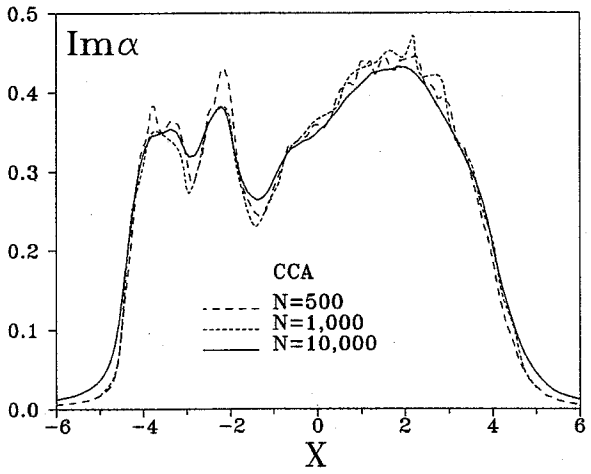

FIG. 1. Absorption spectra, $\mathrm{Im}\alpha(X)$, for cluster-cluster aggregates (CCA's) containing different number of particles, $N=500$, $N=1\,000$, and $N=10\,000$.

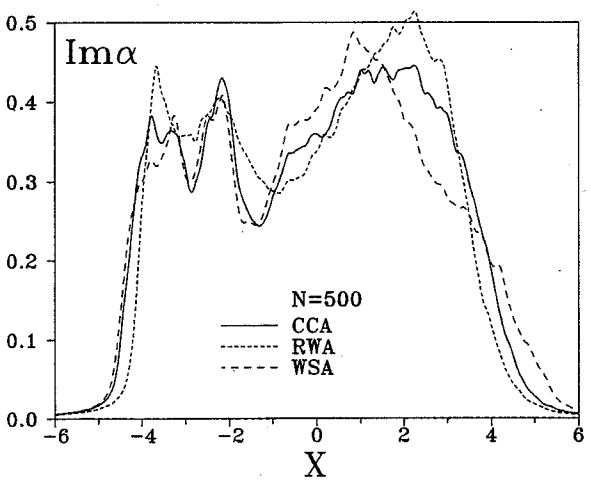

FIG. 2. Absorption spectra, $\mathrm{Im}\alpha(X)$, for various fractals consisting of $N=500$ particles: cluster-cluster aggregates (CCA's), random-walk aggregates (RWA's) and Witten-Sander aggregates (WSA's).

$$N^{-1}\sum_i |d_i|^2=|E_0|^2\mathrm{Im}\alpha/\delta. \tag{17}$$

Taking into account (8)–(13), (15), and (17) one obtains the result that, in the quasistatic approximation, the extinction and the absorption cross sections are equal; equivalently, the scattering cross section is zero. Thus, in order to obtain a nonzero scattering cross section, the first nontrivial correction to the quasistatic solution must be determined, which turns out to be of the order $(k^3/y_a)\sigma_e$.

In general, the decay parameter δ depends on ω. In this section, however, we present our results as functions of $X=X(\omega)$ assuming that $\delta=\mathrm{const}$ (this is the case, in particular, for a two-level system). As was mentioned above, in terms of X, the spectra exhibit a universal behavior since they are determined only by aggregate morphology (and the interaction operator), and do not depend on material properties. Material properties of monomers and the corresponding λ dependence for aggregates of metal particles will be considered in Sec. V.

All quantities below are expressed in units such that the diameter of a particle (equivalent to the lattice period for lattice clusters) is equal to one: $a=1$. (Note that in Refs. 15, 17 and 26, different units, with $R_0=1$, were used; for CCA's, in particular, one has $R_0\approx a/3$.) In the calculations presented in this section the decay constant $\delta=0.1$ for all clusters except those consisting of 10 000 particles, for which we set $\delta=0.2$. The results of simulations were averaged over 10 random cluster realizations for all clusters, except the 10 000 particle CCA's, where the averaging was performed over 4 random realizations.

We now consider the results of our numerical simulations. In Fig. 1, we plot $\mathrm{Im}\alpha$ as a function of X for CCA's with different numbers of particles, $N=500$, 1000 and 10 000. The absorption $\mathrm{Im}\alpha(X)$ exhibits little variation with N; however, the shape of the function is much more complicated than for diluted CCA's (compare with corresponding figures from Refs. 15 and 17). The absorption $\mathrm{Im}\alpha(X)$ in the diluted CCA (DCCA) has one maximum near $X=0$ and is nearly symmetrical. For CCA's there are at least three well-pronounced maxima significantly shifted from $X=0$, and the symmetry is broken. These differences in the spectra of diluted and original clusters arise from the fact that the process of dilution does not conserve the local structure of clusters (although, the global fractal morphology is conserved).

Note that the exact properties for the first two moments of the quasistatic solutions[15]

$$\int \mathrm{Im}\alpha(X)=\pi, \quad \int X\,\mathrm{Im}\alpha(X)dX=0$$

hold for the functions shown in Fig. 1. The higher odd moments of $\mathrm{Im}\alpha(X)$, however, are nonzero.

The three-maxima structure holds for various types of fractal clusters, as can be seen from Fig. 2 where $\mathrm{Im}\alpha(X)$ is plotted for different 500 particle CCA's, WSA's, and RWA's fractal clusters. However, there are shifts in positions of the maxima for different types of clusters (especially, for positive X). For all fractals considered, there is a large inhomogeneous broadening; the absorption is reduced only for $|X|>5$ (while the homogeneous half-width δ is very small, $\delta=0.1$).

The spectral dependence of $\mathrm{Im}\alpha(X)$ for trivial clusters ($D=d=3$) is very much different from those for fractals. In Fig. 3, we plot $\mathrm{Im}\alpha(X)$ for RGP and CPSP with the same number of particles, $N=500$. Both spectra are nearly symmetrical and narrow (the half-width is $\approx 5\ \delta$ for both RGP and CPSP). Thus, in contrast to fractal aggregates, such clusters do not show large inhomogeneous broadening. (In fact, for $a\to 0$ and $N\to\infty$ one anticipates that the spectra in both cases will be similar to those of isolated spherical particles.)

Thus, dipole-dipole interactions in fractals, in contrast to nonfractal composites (sparse, like RGP, or compact, like CPSP), result in a significantly larger inhomogeneous broadening. (In terms of the optical wavelength, the eigenmodes of silver CCA's, for example, span the visible and infrared parts of the spectrum, while modes in nonfractal silver CPSP and RGP are confined to a narrow range between approximately 350 nm and 450 nm.) This results from the fact that, for

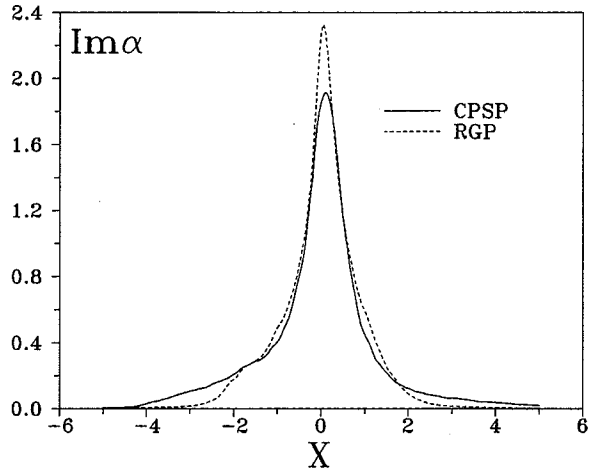

FIG. 3. Absorption spectra for nonfractal 500-particle aggregates: a close-packed sphere of particles (CPSP) and a random gas of particles (RGP).

fractals, the dipole-dipole interaction is not long range, and therefore eigenmodes are localized in small areas of the fractal aggregate; these areas have very different local structures and, accordingly, they resonate at different frequencies. In contrast, in compact nonfractal aggregates (with $D=d=3$), dipolar modes are delocalized over the whole sample, and their eigenfrequencies lie in a narrow spectral interval. We return to discuss this point in Sec. VI.

We next consider scaling properties of $\mathrm{Im}\alpha$. The scaling theory developed in Ref. 15 asserts that, for a fractal cluster, $\mathrm{Im}\alpha(X)$ must, for small $|X|$, exhibit a power-law dependence of the form $|X|^{d_o-1}$; d_o is the optical spectral dimension, which must lie in the interval $0\leq d_o\leq 1$. The same spectral behavior was predicted for the density of eigenstates $\nu(X)$ [i.e., $\mathrm{Im}\alpha(X)\approx\nu(X)$]. The numerical results obtained in Refs. 15 and 17 showed that these predictions are correct for diluted fractal clusters. (Note, however, that because of the strong statistical noise in the simulations,[15,17] the scaling of absorption for DCCA was disputed recently in Ref. 26.) As follows from our simulations (see below), these scaling results fail for nondiluted clusters.

We now give a more detailed discussion of the functional dependence of $\mathrm{Im}\alpha(X)$, for 10 000-particle CCA's (solid line in Fig. 1) for small values of $|X|$. The point $X=0$ can be considered as a special point in the spectral contour. In the range $-1.4\leq X\leq -0.7$, the function $\mathrm{Im}\alpha$ increases with increasing X, approximately following the power-law dependence, $\mathrm{Im}\alpha\propto|X|^{-s}$, with $s=0.34\pm0.01$. In the region near $X=0$, the rate of increase becomes significantly smaller. The absorption again increases in the range $0.4\leq X\leq 1.3$ as a power-law function, $\mathrm{Im}\alpha\propto X^t$, with $t=0.11\pm0.01$. Qualitatively similar behavior for small X was also obtained for RWA and WSA clusters; see Fig. 2. We note that such behavior resembles the dependence of conductivity on $(p-p_c)$ in the vicinity of the percolation threshold p_c (see Ref. 10), where p is the metal volume fraction.

The power-law dependence of the absorption near the "critical" point $X=0$ might be due to scale invariance, similar to the metal-insulator transition in a percolation system. However, despite the fact that power-law dependences can

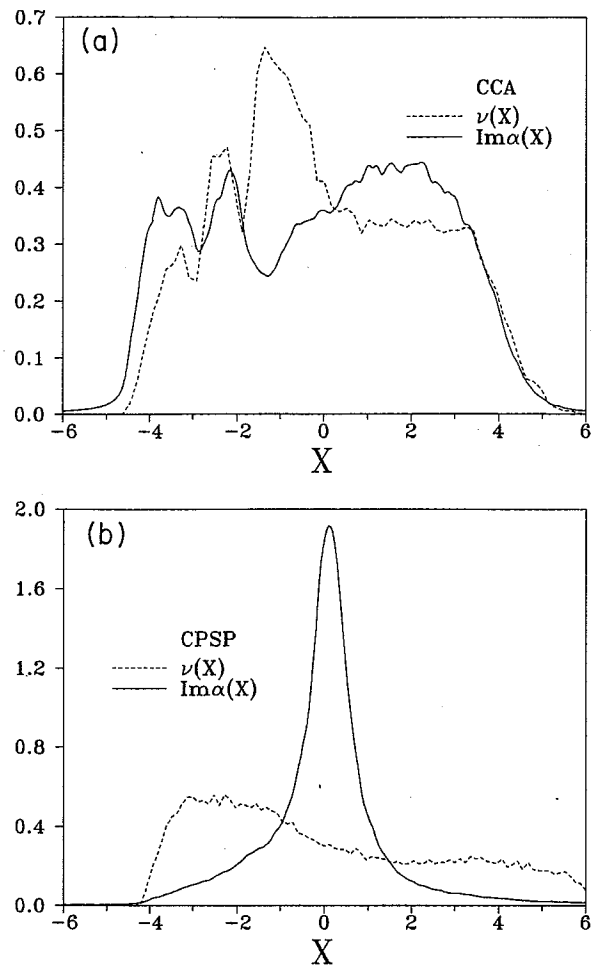

FIG. 4. Spectral dependence of the absorption, $\mathrm{Im}\alpha(X)$, and the density of dipolar eigenmodes, $\nu(X)$, for 500-particle CCA's (a) and CPSP (b).

be deduced for small regions near $X=0$, it must be noted that these regions occupy a very small part of the whole spectrum ($\approx 15\%$ in terms of X). (Therefore, we conclude that convincing evidence of scaling was not observed in our simulations.)

Next we discuss the density of dipolar eigenstates, $\nu(X)=(\pi/3N)dn/dX$, where dn is the number of eigenvalues in the interval dX. The coefficient $\pi/3$ was chosen so that $\nu(X)$ has the same normalization as $\mathrm{Im}\alpha(X)$:

$$\int \nu(X)dX=\pi.$$

Figures 4(a) and 4(b) show the density of eigenstates $\nu(X)$ and $\mathrm{Im}\alpha(X)$ for 500 particle CCA's and CPSP, respectively. It is apparent from Fig. 4(a) that the distribution of eigenmodes in CCA's is not symmetrical and differs significantly from $\mathrm{Im}\alpha(X)$. This implies that selection rules are of importance and the density of eigenstates itself does not determine $\mathrm{Im}\alpha(X)$. Thus, the conclusion of Refs. 15, 16, and 26 that $\mathrm{Im}\alpha(X)\approx\nu(X)$ is, in general, not correct and different modes of CCA's contribute to $\mathrm{Im}\alpha(X)$ with different weights, in contrast to DCCA. The greatest difference in $\mathrm{Im}\alpha$ and ν is near the point $X=-1$. Whereas $\nu(X)$ has a

maximum near this point, Imα has, by way of contrast, a minimum. [It is worth noting that a pair of monomers separated by unit distance has an eigenstate with $w=-1$ which is antisymmetric (total dipole moment zero) with polarization orthogonal to the line connecting the monomers.[32]]

As follows from Fig. 4(b) the difference between Im $\alpha(X)$ and $\nu(X)$ is especially large for random CPSP. This result was anticipated for the following reason. For a continuous dielectric sphere, there is only one dipole eigenstate with nonzero total dipole moment (i.e., the selection rules are of great importance); since the CPSP can be considered as a discrete model for such a sphere, we conclude that selection rules are important in CPSP. Thus, despite the fact that our calculations demonstrate the significance of selection rules for CCA's, their role there is not as important as for the case of trivial aggregates, such as CPSP. In particular, as follows from Fig. 4(a), almost all eigenmodes within the interval $|X|<5$ contribute significantly to the absorption.

We finally consider the localization length, $L(w_n)\equiv L_n$, characterizing a quasistatic eigenstate $|n)$. The $3N$ projections of the $|n)$ vector on the orthonormal basis $|i\alpha)$ determine its spatial behavior. The weight with which the nth eigenstate is localized on the ith monomer is given by $m_n(\mathbf{r}_i)\equiv m_n(i)=\Sigma_\alpha[(i\alpha|n)]^2$; they are normalized by the condition $\Sigma_i m_n(i)=1$. In terms of these weights, the localization length L_n of the nth eigenmode is defined as:[15,18]

$$L_n\equiv L(w_n)=\sum_{i=1}^{N} m_n(i)\mathbf{r}_i^2-\left(\sum_{i=1}^{N} m_n(i)\mathbf{r}_i\right)^2. \tag{18}$$

This formula is actually a discrete function of its argument w_n. One can obtain a smooth localization function $L(X)$ by averaging $L(w_n)$ over a given interval ΔX for an ensemble of clusters

$$L(X)=\left\langle [K(X,\Delta X)]^{-1}\sum L(w_n)\right\rangle, \tag{19}$$

where the summation is taken over all n satisfying the condition $|X-w_n|\leq\Delta X$, and $K(X,\Delta)$ is the number of terms in this sum. The symbol $\langle\cdots\rangle$ denotes an average over an ensemble of random clusters.

In Fig. 5 we present the results of our simulations for $L(X)$ for 500-particle CCA's ($\Delta X\approx 0.6$). The points indicate values of the original function $L(w_n)$ for one particular cluster while the solid line shows the result of averaging over 10 random cluster realizations.

From Fig. 5, we see that $L(X)$ exhibits large fluctuations, especially near the central point $X=0$. There are modes that are strongly localized and those that are delocalized. The mode localization increases, on average, toward large values of $|X|$, so that for the most localized modes $L(X)$ reduces to a dimension comparable to the size of a monomer, a.

V. WAVELENGTH-DEPENDENT DIPOLE INTERACTION IN SILVER COMPOSITES: NUMERICAL SIMULATIONS AND EXPERIMENTAL DATA

In this section, we specify the dependence $\alpha_0(\lambda)$ and also calculate the optical cross-section as a function of the wavelength for silver colloid aggregates. The results of our simulations will be compared with experimental data.

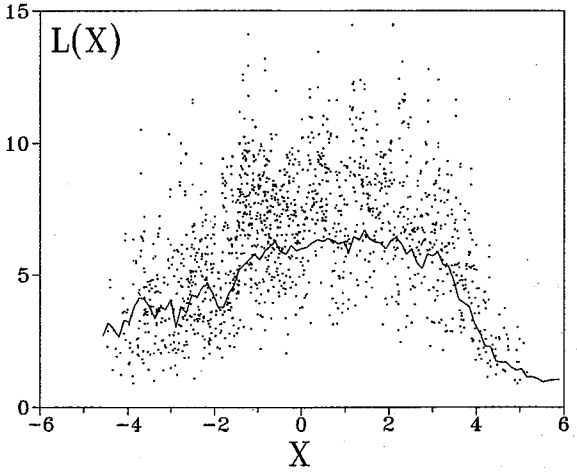

FIG. 5. The localization length, $L(X)$, of dipole eigenmodes vs their eigenvalues X for 500-particle CCA's. The dependence $L(X)$ averaged over an interval of $\Delta X=0.6$ for 10 random cluster realizations is shown by the solid line.

An expression for the dipole polarizability of a dielectric sphere of radius R_m, which takes into account the radiation reaction correction, has the form:[29]

$$\alpha_0=R_m^3\frac{\epsilon-\epsilon_h}{\epsilon+2\epsilon_h-i(2/3)(kR_m)^3(\epsilon-\epsilon_h)}, \tag{20}$$

where $\epsilon=\epsilon'+i\epsilon''$ is the dielectric function of the particle material (silver, in our case) and ϵ_h is the dielectric constant of a host medium, which we assume to be water. The dielectric constant of water is assumed to be real (we neglect the small absorption in water) and nearly constant, $\epsilon_h\equiv\epsilon_w=1.78$, in the spectral range under consideration (from 200 to 1000 nm).

The radiation correction introduced above results in the expression for α_0 satisfying the optical theorem and the energy conservation law. From (10), (15), and (20) one obtains for $\delta=-\mathrm{Im}\alpha_0^{-1}$ and $X=-\mathrm{Re}\alpha_0^{-1}$ the following expressions:

$$\delta=R_m^{-3}\frac{3\epsilon_h\epsilon''}{|\epsilon-\epsilon_h|^2}+2k^3/3,\quad y_a=R_m^{-3}\frac{3\epsilon_h\epsilon''}{|\epsilon-\epsilon_h|^2}>0, \tag{21}$$

and

$$X=-R_m^{-3}\left(1+\frac{3\epsilon_h(\epsilon'-\epsilon_h)}{|\epsilon-\epsilon_h|^2}\right). \tag{22}$$

The dielectric function in a metal is well-described by the Drude formula

$$\epsilon=\epsilon_0-\frac{\omega_p^2}{\omega(\omega+i\gamma)}, \tag{23}$$

where ϵ_0 includes the contribution to the dielectric constant associated with interband transitions in bulk material, ω_p is the plasma frequency and γ is the relaxation constant. In our calculations, we used the optical constants of bulk silver tabulated as a function of λ in Ref. 38. The data were modi-

fied to take into account finite size effects in small metallic spheres (wall scattering). The radius-dependent dielectric function, $\epsilon(R_m)$, was obtained from the relation $\epsilon(R_m) = \epsilon_{\text{tab}} + \omega_p^2/[\omega(\omega + i\gamma_\infty)] - \omega_p^2/[\omega(\omega + i\gamma(R_m))]$, where ϵ_{tab} are the tabulated data[38] for the dielectric constant in the bulk silver, γ_∞ is the bulk relaxation constant, and the radius-dependent relaxation, $\gamma(R_m)$, is given by $\gamma(R_m) = \gamma_\infty + v_F/R_m$, with v_F the Fermi velocity. For silver $\lambda_p = 2\pi c/\omega_p = 136.1$ nm, $\gamma_\infty/\omega_p = 0.0019$, and $v_F/c = 0.0047$.

To simulate the silver colloid aggregates studied in our experiment, we used the CCA model described in Sec. III. CCA have fractal dimension, structure, and aggregation pattern very similar to those observed in the experiment. This model contains two adjustable parameters, the lattice period, a, which defines the relative distances, r_{ij}, between particles, and the radius of a monomer, R_m. Clearly, solutions of the CDE's are very sensitive to the ratio a/R_m, because this parameter determines the interaction strength. The model of geometrically touching spheres, which seems to be the most natural, implies that $a/R_m = 2$. However, as was shown in Ref. 39, this model fails to describe the long-wavelength resonances observed in a group of particles; it also fails to describe the long-wavelength tail observed in the absorption spectra of colloid aggregates (see, for example, Refs. 23 and 30).

The physical reason for the failure of this model is that the dipole approximation is not strictly applicable for touching spheres.[39–43] Indeed, the dipole field produced by one of the touching monomers is highly inhomogeneous ($\propto r^{-3}$) within the volume of the other one. This inhomogeneous field should result in high-order multipole moments, coupled both to each other and to the incident field. The high-order moments, when they are taken into account, effectively increase depolarization factors, and lead to the low-frequency resonances observed in experiments.[39] However, incorporating these high-order moments into the calculation results in an essentially intractable problem for the large fractal clusters considered here.

As suggested by Purcell and Pennypacker,[44] and developed by Draine,[29] a description of the optical response of an arbitrary shaped object can be obtained, remaining within the dipole approximation. (It is worth noting that the macroscopic Maxwell equations also contain only dipolar terms, i.e., polarization.) Below we generalize these ideas for fractal aggregates.

To account for multipolar effects in the CDE's, following Refs. 7 and 32, real touching spheres may be replaced by effective spheres which geometrically intersect. Formally, this requires the ratio a/R_m to be taken less than 2. The physical reason underlying this procedure can be understood from the following arguments. Consider a pair of touching spheres and ascribe to the first sphere a dipole moment d located at its center. Since we would like to remain within the dipole approximation, the second sphere should also be replaced by a point dipole located at a certain distance from the first sphere. Clearly, because the field associated with the first sphere decreases nonlinearly, $\sim d/r^3$, the second dipole should be placed somewhere closer than $2R_m$ from the center of the first sphere (otherwise, the interaction between the spheres would be underestimated). In other words, in order to correctly describe the interaction between the spheres remaining within the dipolar approximation, the distance between the dipoles must be taken less than $2R_m$. This is equivalent to replacing the original touching spheres by overlapping spheres with the dipole moments located at their centers.

To gain insight concerning selection of the ratio a/R_m, we first consider cases for which a/R_m is known exactly. As shown in Refs. 29, 44, and 45, the correct description of the optical response of a small object of arbitrary shape was obtained by considering dipolar interactions of a set of spherical monomers placed on a simple cubic lattice inside the volume of the object; the lattice period, a, was chosen such that $a^3 = (4\pi/3)R_m^3$. This relation which provides equality of the total volume of the spheres and the original object under consideration, gives the ratio $a/R_m = (4\pi/3)^{1/3} \approx 1.612$. In Ref. 46 it was shown that, within the dipole approximation, correct depolarization coefficients for a linear array of spherical monomers are obtained provided a/R_m is chosen to be $(4\zeta_3)^{1/3} \approx 1.688$ ($\zeta_3 = \Sigma_k k^{-3}$), i.e., close to the above-mentioned value. We used $a/R_m = (4\pi/3)^{1/3}$ in our calculations.

We also required that the radius of gyration and the total mass of clusters used in simulations must be the same as in the experiment. This condition, combined with $a/R_m = (4\pi/3)^{1/3}$, can be satisfied for fractals ($D \neq 3$) if one chooses $R_m = R_{\text{expt}}(\pi/6)^{D/[3(3-D)]}$, where R_{expt} is the radius of monomers used in experiments. In our experiments described below, the radius of silver particles forming colloidal aggregates was $R_{\text{expt}} \approx 7$ nm, so that $R_m \approx 5$ nm for $D = 1.78$.

For a light beam propagating in a system, which contains randomly distributed clusters far away from each other (so that the clusters do not interact), the intensity dependence is given by the expression $I(z) = I(0)\exp(-\sigma_e \rho z)$; the cluster density, $\rho = p/[(4\pi/3)R_{\text{expt}}^3\langle N\rangle]$, where p is the volume fraction filled by spherical particles. Introducing the extinction efficiency Q_e by the known relation

$$Q_e = \frac{\langle \sigma_e \rangle}{\langle N \rangle \pi R_{\text{expt}}^2} = \frac{4k\ \text{Im}\alpha}{R_{\text{expt}}^2}, \tag{24}$$

the intensity dependence $I(z)$ acquires the form

$$I(z) = I(0)\exp\left(-\frac{3}{4}Q_e p(z/R_{\text{expt}})\right). \tag{25}$$

As follows from (25), the extinction efficiency Q_e is a quantity that is measured in experiments on light transmission (rather than σ_e).

In Fig. 6(a) and 6(b) we plot the frequency variable X and relaxation parameter δ defined in (21) and (22) against wavelength (for $a^3/R_m^3 = 4\pi/3$ and $R_m = 5$ nm). For values of $\epsilon = \epsilon(\lambda)$ in (21) and (22), we used $\epsilon(R_m)$ found from the experimental data of Ref. 38, which were modified to take into account finite-size effects (see above). The structures seen in Fig. 6, for wavelengths below 300 nm, are basically due to interband transitions. The λ dependence of X and δ near 400 nm, and toward longer wavelengths, are associated with surface plasmon resonances. As seen in Fig. 6(a), X changes significantly from 400 nm to 800 nm; hence, differ-

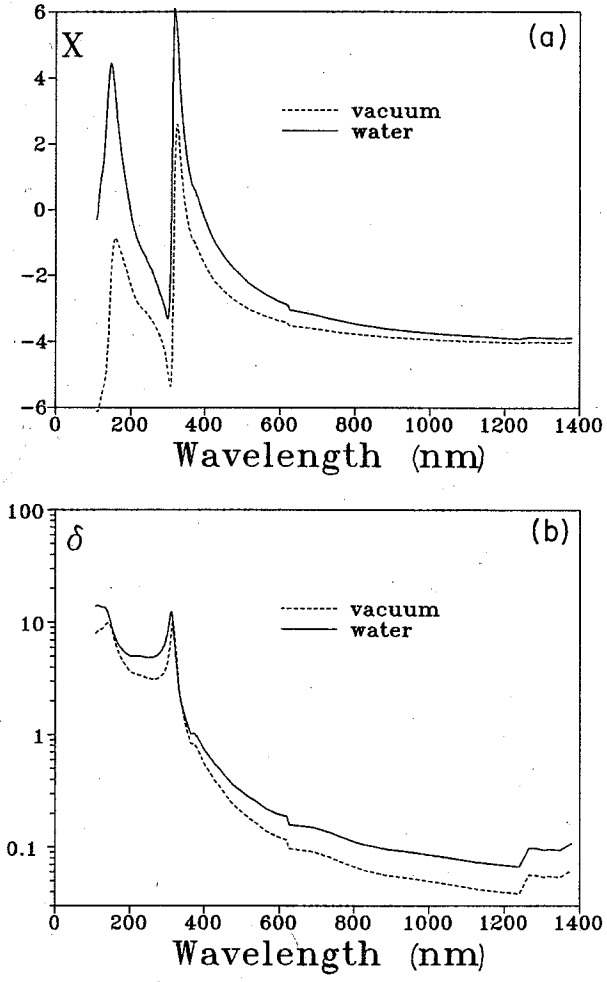

FIG. 6. The spectral variable X (a) and decay constant δ (b) vs wavelength for fractal aggregates of 7 nm radius silver particles in vacuum and water.

ent dipole eigenmodes of a cluster can be excited by an applied field at different λ. In the long-wavelength region, from 800 nm toward longer wavelengths, X is almost constant ($X \approx X_0 = -a^3/R_m^3 = -4\pi/3$). This means that a change in λ in this region does not change the resonant dipole mode, which can be referred to as the "zero-frequency mode," or more simply as the "zero-mode." (Note, however, that, whereas $X \approx$ const for $\lambda > 800$ nm, the relaxation constant δ significantly decreases from 800 nm towards the longer wavelengths, leading to increased resonance quality factor.) Since, in the long-wavelength region, the value of X (and, therefore, the mode excited) does not change with λ, the corresponding local field distribution in a cluster is also independent of the wavelength.

The enhanced far-infrared absorption, generally attributed to clustering, can be related to the excitation of the zero mode of a cluster. Interactions between particles aggregated into a cluster lead to the formation of eigenmodes, including the zero mode. The latter mode occurs in the long-wavelength part of the spectrum, where $X(\lambda) \approx X_0$ for all λ. When the cluster is excited by a low-frequency applied field, so that $X(\omega) \approx X_0$, absorption is primarily due to zero-mode excitation and is large because of its resonant character. For nonaggregated, well-separated particles, the absorption spectrum is centered in the narrow region near the center $X(\lambda_0) = 0$ (e.g., $\lambda_0 \approx 400$ nm for silver particles in water); therefore, there are no resonances in the long-wavelength part of the spectrum, where $X(\lambda) \approx X_0$, and, therefore, the absorption is small. Thus, the zero-mode formation, which accompanies particle clustering, results in the enhanced far-infrared absorption.

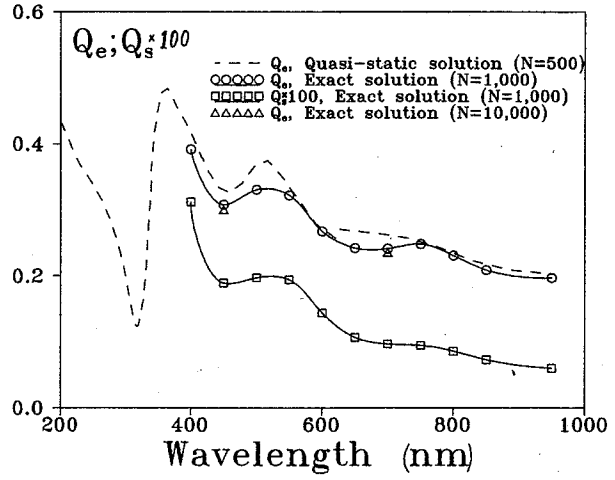

FIG. 7. Extinction efficiency Q_e and scattering efficiency Q_s vs wavelength. Q_e is calculated in the quasistatic approximation for 500-particle CCA's and on the basis of the exact dipolar interaction for 1000 particle and 10 000-particle CCA's. Q_s is calculated for 1000-particle CCA's with the exact dipole interaction.

Provided the dependences $X = X(\lambda)$ and $\delta = \delta(\lambda)$ are specified, one can express the solutions of the CDE's [expressed in terms of X and δ; see Eqs. (6)–(15)] as explicit functions of wavelength.

In Fig. 7, we plot the extinction efficiency Q_e as a function of λ, calculated on the basis of the exact and quasistatic dipolar interaction. The solution in the quasistatic limit was obtained by the Jacobi diagonalization method for 500 particle clusters. The solution of the CDE's with the exact dipolar interaction (2)–(4) was obtained by the conjugate gradient method for 1 000 particle clusters (for a control we also calculated Q_e at two different wavelengths for 10 000 particle clusters). As seen in the figure, these solutions are in good agreement. It was shown in Ref. 17, that the quasistatic approximation is, under certain conditions, a good approximation for the description of dipolar excitations on fractals. This occurs because most eigenmodes are localized in areas smaller than the wavelength λ, and, accordingly, the contributions to the local field of dipoles located at distances that are comparable with or larger than λ are of no importance.

In Fig. 7, we also present the scattering efficiency $Q_s = \langle \sigma_s \rangle / [\langle N \rangle \pi R_{\text{expt}}^2]$, where the scattering cross section σ_s is given by $\sigma_s = \sigma_e - \sigma_a$ [σ_e and σ_a are defined by (8) and (9)]. As follows from the figure, the scattering is small so that in this case $\sigma_e \approx \sigma_a$.

We also performed experiments to study extinction in silver colloid aggregates. Fractal aggregates of silver colloid particles were produced from a silver sol generated by reducing silver nitrate with sodium borohydride.[34] The color of fresh (nonaggregated) colloidal solution is opaque yellow;

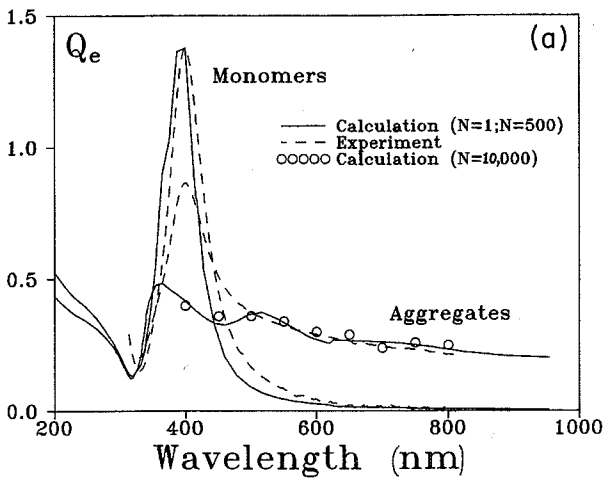

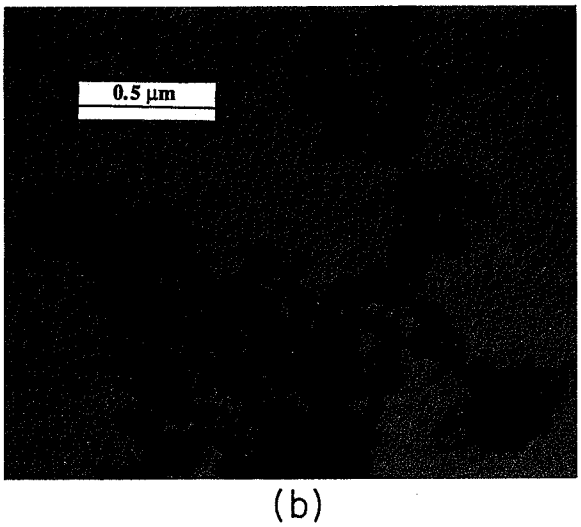

FIG. 8. (a) Experimental and calculated extinction spectra of silver colloid CCA's. The theoretical spectra are presented for 500-particle and 10 000-particle CCA's. (b) Electron micrograph of a typical silver colloid aggregate.

the corresponding extinction spectrum [see Fig. 8(a)] is peaked at 400 nm with the half-width about 40 nm. Addition of adsorbent (fumaric acid) promotes aggregation and fractal colloid clusters formed. When adding the fumaric acid (0.1 cm^3 of 0.5M aqueous solution) into the colloids (2.0 cm^3), the color of colloids changes through dark orange and violet to dark grey over 10 h. A broad wing in the long-wavelength part of the extinction spectrum appears after aggregation, as seen in Fig. 8(a). The spectra were taken using a Hewlett Packard 8452A diode array spectrometer.

An electron micrograph of a typical silver colloid aggregate is shown in Fig. 8(b). The process of formation of such an aggregate can be summarized as follows (see also Sec. III). A large number of initially isolated silver nanoparticles execute random walks in the solution. Encounters with other nanoparticles result in their sticking together, first to form small groups, which then aggregate into larger formations, and so on. Such cluster-cluster aggregation,[33] readily simulated by a computer, results in clusters with fractal dimension $D \approx 1.78$, corroborated by measurements of D for silver colloid aggregates such as that shown in Fig. 8(b).

Experimental extinction spectra were compared with numerical simulations in Fig. 8(a). The calculations were performed for 500-particle CCA's (solid line with a large wing) and for 10 000-particle CCA's (circles). For comparison, the experimental spectra and numerical results for nonaggregated monomers are also presented in the figure. Clearly, the aggregation results in a large tail in the red and infrared part of the spectrum, which is well described by the simulations. The discrepancy in the central part of the spectrum probably occurs because, in the experiments, a number of particles remained nonaggregated and led to additional (not related to fractal aggregate) absorption near 400 nm. However, we cannot rule out the possibility that the discrepancy would be eliminated if one took all higher multipole moments into account (i.e., exactly, as opposed to introducing intersecting spheres).

VI. CONCLUDING DISCUSSION

Below we briefly summarize our results and offer some concluding remarks.

We first discuss dipolar excitations in the quasistatic limit. As is well known, there is only one dipolar mode that can be excited by a homogeneous field in a spherical particle (in a spheroid there are three dipole modes). For a three-dimensional collection of small particles, such as the random close-packed sphere of particles (CPSP) and the random gas of particles (RGP), the absorption spectra are still peaked near the relatively narrow surface plasmon resonance of the individual particles, i.e., all eigenmodes of the collection of particles are located in a small spectral interval (see Fig. 3).

In contrast to conventional three-dimensional systems, the dipolar interaction in low-dimensional fractals is not long range, which results in localization of the corresponding eigenmodes (see Fig. 5) at various random locations in the cluster. These modes form the optical spectrum of fractal aggregates which is characterized by strong inhomogeneous broadening. It is important to note that, despite the asymptotically zero density of particles in a fractal cluster, there is always a high probability ($\propto r^{D-3}$) of finding a number of particles in close proximity to any given one. Therefore, there are strong interactions between neighboring particles, which lead to the formation of eigenmodes covering a broad spectral range (i.e., the large variety of different local configurations in a fractal cluster leads to the wide spectral interval covered by the eigenmodes). We emphasize that this behavior is different from nonfractal RGP and CPSP, where dipolar modes occupy a narrow spectral interval.

Thus, fractality provides a strong inhomogeneous broadening (and, hence, resonant modes covering a wide spectral range) in a collection of particles interacting via dipolar forces. Neither RGP nor CPSP provide such broadening (compare Figs. 1 and 2 with Fig. 3). For example, eigenmodes of silver RGP and CPSP lie in the small region between approximately 350 nm and 450 nm, whereas modes in silver fractal colloid aggregates cover a large spectral interval including the visible and infrared parts of the spectrum. (Note that for any λ in the long-wavelength part of the spectrum, a single "zero mode" is in resonance with the applied field.) It is also important that modes located towards the red and infrared part of the spectrum possess larger quality-

factor $\propto \delta^{-1}$[see Eqs. (21) and (23)] and therefore local fields associated with their excitation are especially large.

Our experimental studies of light extinction in silver colloid fractal aggregates are in good agreement with the results of numerical simulations, except for the central peak [see Fig. 8(a)].

In extended (larger than the wavelength) three-dimensional objects dipolar excitations are typically running plane waves (polaritons) which are eigenmodes of the operator of translational invariance. In contrast, fractals do not possess translational invariance (they are scale invariant), and the dipolar eigenmodes are localized (see Fig. 5). Because of the fact that localization occurs in areas that are smaller than the wavelength, optical spectra of fractal clusters that are larger than the wavelength look similar to those for clusters that are smaller than the wavelength (see Fig. 7).

The theory of Ref. 15 predicted a scaling behavior for absorption spectra of fractals. While the predicted scaling was previously obtained for diluted clusters, the optical properties of original, nondiluted, clusters do not show convincing evidence of scaling. A possible reason for the absence of strong scaling may be related to the fact that for all values of X there are modes that are sufficiently localized (see Fig. 5) that only a few particles are involved in the excitation, and scale invariance does not manifest itself distinctively for such small distances. Another possible reason is due to symmetry properties of the eigenmodes. As our simulations show, eigenmodes are strongly asymmetric in contrast to the assumption of Ref. 15 of the spherical, on average, symmetry of modes. Scaling in this case might occur individually for modes with a certain degree of asymmetry (some effective "aspect ratio") while the overall spectrum, formed from modes of different symmetries, may exhibit multifractal scaling.

As follows from Fig. 4(a), absorption does not really follow the spectral density of eigenstates, as was stated in Refs. 15, 16, and 26 (i.e., different modes contribute to the spectrum with different weights). This result is probably related to the above-mentioned asymmetry of dipolar eigenmodes in fractals and to corresponding selection rules for the absorption. However, we note that the difference between the absorption and the density of states for random fractals is not as large as for the case of non-fractal aggregates, such as CPSP [see Fig. 4(b)].

ACKNOWLEDGMENTS

Work at NMSU was supported in part by NSF under Grant No. DMR-9500258 and by NATO under Grant No. CRG 950097. Work at Sandia was supported by the United States Department of Energy under Contract No. DE-AC04-94AL85000.

APPENDIX

Consider a symmetric matrix $\hat{V}$ of order q ($q=3N$ in our case, where N is the number of particles) with complex components. First we assume that $\hat{V}$ is not degenerate. In this case its eigenvectors $|n)$ $(n=1,\ldots,q)$ form a (normalized) basis in C^q space.[47] We also introduce a basis of unit vectors $|e_i)$ $(i=1,\ldots,q)$ which are vectors with unit entry in the ith position and zeros in all other positions. The symmetry of $\hat{V}$ means that $(e_i|\hat{V}|e_j)=(e_j|\hat{V}|e_i)$ for any i and j.

The eigenvectors of a complex symmetric matrix $\hat{V}$ (in contrast to a Hermitian matrix) are not, in general, orthogonal, i.e., $(m|n)\neq\delta_{mn}$. The "orthogonality rule" is replaced in this case by

$$(\bar{m}|n)=0 \quad (m\neq n), \tag{A1}$$

where $|\bar{n})$ is obtained from $|n)$ by complex conjugation of all components (but without transposition). Thus, if $|n)$ is a column vector, then $(\bar{n}|$ is a row vector with the same entries as $|n)$.

To prove (A1), we consider $(\bar{n}|\hat{V}|m)$:

$$(\bar{n}|\hat{V}|m)=\sum_{ij}(\bar{n}|e_i)(e_i|\hat{V}|e_j)(e_j|m). \tag{A2}$$

Noting that $(\bar{n}|e_i)=(e_i|n),(e_j|m)=(\bar{m}|e_j)$, and $(e_i|\hat{V}|e_j)=(e_j|\hat{V}|e_i)$, we obtain

$$(\bar{n}|\hat{V}|m)=\sum_{ij}(\bar{m}|e_j)(e_j|\hat{V}|e_i)(e_i|n)=(\bar{m}|\hat{V}|n). \tag{A3}$$

On the other hand, we have $(\bar{n}|\hat{V}|m)=v_m(\bar{n}|m)$ and $(\bar{m}|\hat{V}|n)=v_n(\bar{m}|n)$, where v_n and v_m are the eigenvalues of $\hat{V}$. Since $v_n\neq v_m$, the equality (A3) can hold only if $(\bar{n}|m)=(\bar{m}|n)=0$; this proves (A1).

Representation of the unit matrix in the introduced basis is $\hat{I}=\Sigma[(\bar{n}|n)]^{-1}|n)(\bar{n}|$.

Now we derive formula (6) for the solution of Eq. (5). Since the eigenvectors of $\hat{V}$ form a complete basis in C^q, we can decompose $|d)$ over $|n)$

$$|d)=\sum_n c_n|n), \tag{A4}$$

with coefficients c_n. Substituting (A4) into (5) and multiplying both sides of the equation by $(\bar{m}|$, we obtain

$$c_n=\frac{(\bar{n}|E)}{(\bar{n}|n)}\frac{1}{Z+v_n}. \tag{A5}$$

This expression combined with (A4) proves formula (6).

If there is a degenerate state due to a spatial symmetry, the degenerate eigenvectors correspond to some rotations and reflections in three-dimensional space and can be always chosen to satisfy (A1).

*Also with the Institute of Automation and Electrometry, Siberian Branch of the Russian Academy of Science, 630090 Novosibirsk, Russia.

†Author to whom all correspondence should be sent. Also with the L. V. Kirensky Institute of Physics, Siberian Branch of the Russian Academy of Science, 660036 Krasnoyarsk, Russia.

[1] *Electron Transport and Optical Properties of Inhomogeneous Media*, edited by J. C. Garland and D. B. Tanner (AIP, New York, 1978); *Electron Transport and Optical Properties of Inhomogeneous Media (ETOPIM 3)*, edited by W. L. Mochan and R. G. Barrera (North-Holland, Amsterdam, 1994).

[2] B. B. Mandelbrot, *The Fractal Geometry of Nature* (Freeman, San Fransisco, 1982); B. Sapoval, *Fractals* (Aditech, Paris, 1990).

[3] *Fractals & Disorder*, edited by Armin Bunde (North-Holland, Amsterdam, 1992); S. Alexander and R. Orbach, J. Phys. (Paris) Lett. **43**, L1625 (1982).
[4] For a spheroid, there are three resonances with nonzero total dipole moment.
[5] V. M. Shalaev, and M. I. Stockman, Z. Phys. D **10**, 71 (1988).
[6] A. V. Butenko, V. M. Shalaev, and M. I. Stockman, Z. Phys. D **10**, 81 (1988).
[7] V. M. Shalaev, V. A. Markel, and V. P. Safonov, Fractals **2**, 201 (1994); V. M. Shalaev, R. Botet, D. P. Tsai, J. Kovacs, and M. Moskovits, Physica A **207**, 197 (1994).
[8] M. V. Berry and I.C. Percival, Opt. Acta **5**, 577 (1986).
[9] I. H. Zabel and D. Stroud, Phys. Rev. B **46**, 8132 (1992); X. Zhang and D. Stroud, *ibid.* **48**, 6658 (1993); *ibid.* **49**, 944 (1994); P. M. Hui and D. Stroud, *ibid.* **49**, 11729 (1994).
[10] D. J. Bergman and D. Stroud, *Physical Properties of Macroscopically Inhomogeneous Media*, Solid State Physics Vol. 46 (Academic Press, New York, 1992), p. 147.
[11] F. Claro and R. Fuchs, Phys. Rev. B **44**, 4109 (1991); K. Ghosh and R. Fuchs, *ibid.* **38**, 5222 (1988).
[12] R. P. Devaty, Phys. Rev. B **44**, 593 (1991).
[13] F. Brouers *et al.*, Phys. Rev. B **49**, 14582 (1994); **47**, 666 (1993).
[14] G. A. Niklasson, J. Appl. Phys. **62**, R1 (1987).
[15] V. A. Markel, L. S. Muratov, M. I. Stockman, and T. F. George, Phys. Rev. B **43**, 8183 (1991); M. I. Stockman, L. N. Pandey, L. S. Muratov, and T. F. George, Phys. Rev. Lett. **72**, 2486 (1994).
[16] M. I. Stockman, T. F. George, and V. M. Shalaev, Phys. Rev. B **44**, 115 (1991).
[17] V. M. Shalaev, R. Botet, and R. Jullien, Phys. Rev. B **44**, 12216 (1991); **45**, 7592(E) (1992).
[18] V. M. Shalaev, R. Botet, and A. V. Butenko, Phys. Rev. B **48**, 6662 (1993).
[19] M. I. Stockman, V. M. Shalaev, M. Moskovits, R. Botet, and T. F. George, Phys. Rev. B **46**, 2821 (1992).
[20] V. M. Shalaev, M. Moskovits, A. A. Golubentsev, and S. John, Physica A **191**, 352 (1992).
[21] V. M. Shalaev and R. Botet, Phys. Rev. B **50**, 12987 (1994).
[22] S. G. Rautian, V. P. Safonov, P. A. Chubakov, V. M. Shalaev, and M. I. Stockman, Pis'ma Zh. Éksp. Teor. Fiz. **47**, 243 (1988) [JETP Lett. **47**, 243 (1988)].
[23] A. V. Butenko *et al.*, Z. Phys. D **17**, 283 (1990); A. V. Karpov, *et al.*, Pis'ma Zh. Éksp. Teor. Fiz. **48**, 528 (1988) [JETP Lett. **48**, 571 (1988)].
[24] V. M. Shalaev, M. I. Stockman, and R. Botet, Physica A **185**, 181 (1992).
[25] D. P. Tsai, J. Kovacs, Z. Wang, M. Moskovits, V. M. Shalaev, J. Suh, and R. Botet, Phys. Rev. Lett. **72**, 4149 (1994).
[26] M. I. Stockman, L. N. Pandey, L. S. Muratov, and T. F. George, Phys. Rev. B **51**, (1995).
[27] A diluted cluster is obtained by random removal of monomers from the cluster and successive reduction in cluster size, so that the average distance between nearest neighbors remains the same as in the original cluster. This procedure leads to improved spatial scaling at small distances while the global fractal morphology of the cluster remains unchanged (Ref. 15).
[28] D. J. Bergman and D. Stroud, Phys. Rev. B **22**, 3527 (1980); D. J. Bergman and K.-J. Dunn, *ibid.* **45**, 13262 (1992).
[29] B. T. Draine, Astrophys. J. **333**, 848 (1988).
[30] Yu. E. Danilova, V. A. Markel, and V. P. Safonov, Atmos. Oceanic Opt. **6**, 821 (1993).
[31] As was shown in Ref. 32, if the condition $y_a \gg 2k^3/3$ is not fulfilled, the quasistatic approximation fails no matter how small the cluster size.
[32] V. A. Markel, J. Mod. Opt. **39**, 853 (1992).
[33] R. Jullien and R. Botet, *Aggregation and Fractal Aggregates* (World Scientific, Singapore, 1987); P. Meakin, Phys. Rev. Lett. **51**, 1119 (1983); M. Kolb, R. Botet, and R. Jullien, *ibid.* **51**, 1123 (1983).
[34] D. Weitz and M. Oliveria, Phys. Rev. Lett. **52**, 1433 (1984); J. A. Creighton, in *Surface Enhanced Raman Scattering*, edited by R. K. Chang and T. E. Furtak (Plenum Press, New York, 1982).
[35] T. A. Witten and L. M. Sander, Phys. Rev. B **27**, 5686 (1983).
[36] J. K. Collum and R. A. Willoughby, *Lanczos Algorithm for Large Symmetric Eigenvalue Computations* (Birkhäuser, Boston, 1985), Vol. 1.
[37] *Solid State Physics* (Academic Press, New York, 1980), Vol. 35.
[38] *Handbook of Optical Constants of Solids*, edited by E. D. Palik (Academic Press, New York, 1985).
[39] J. E. Sansonetti and J. K. Furdyna, Phys. Rev. B **22**, 2866 (1980).
[40] M. Ausloos, P. Clippe, and A. A. Lucas, Phys. Rev. B **18**, 7176 (1978).
[41] P. Clippe, R. Evrard, and A. A. Lucas, Phys. Rev. B **14**, 1751 (1976).
[42] J. M. Gerardy and M. Ausloos, Phys. Rev. B **22**, 4950 (1980).
[43] F. Claro, Solid State Commun. **29**, 229 (1984).
[44] E. M. Purcell and C. R. Pennypacker, Astrophys. J. **186**, 705 (1973).
[45] S. B. Singham and C. F. Bohren, J. Opt. Soc. Am. A **5**, 1867 (1988).
[46] V. A. Markel, J. Mod. Opt. **40**, 2281 (1993).
[47] Roger A. Horn and Charles A. Johnson, *Matrix Analysis* (Cambridge University Press, Cambridge, 1985).